
UNDERSTANDING PRUNING REGIMES IN VISION-LANGUAGE MODELS THROUGH DOMAIN-AWARE LAYER SELECTION

Saeed Khaki
Microsoft AI
saeedkhaki@microsoft.com

Nima Safaei
Ohio State University
safaei.3@osu.edu

Kamal Ginotra
Microsoft AI
kamalginotra@microsoft.com

March 24, 2026

ABSTRACT

Transformer-based vision-language models (VLMs) contain substantial depth redundancy, yet the effect of removing specific decoder layers remains poorly understood, especially for domains that require tight coupling between perception and multi-step reasoning. We study structured decoder layer pruning through the lens of *domain-aware activation similarity*, measuring how strongly each layer transforms representations for math versus non-math inputs. This yields simple math-aware, non-math-aware, and mixed ranking criteria that identify layers whose input–output activations change least within a target domain. Across two state-of-the-art VLMs and a broad suite of math and general multimodal benchmarks, we uncover a consistent three-regime structure: at low pruning budgets, performance is highly sensitive to which layers are removed; at moderate budgets, methods converge as structural damage accumulates; and at high budgets, structural continuity dominates, favoring spacing-aware strategies. Our domain-aware rankings achieve the strongest stability in the ranking-sensitive regime, while matching or exceeding structure-aware baselines at larger budgets. These results provide a clearer picture of how depth contributes to domain-specific behavior in VLMs and offer a practical, interpretable approach to reducing model depth without sacrificing essential mathematical or general vision-language capabilities.

1 Introduction

Vision-language models (VLMs) have become a practical foundation for multimodal assistants, combining strong visual perception with open-ended language generation and instruction following. Modern systems typically pair a visual encoder with an autoregressive transformer decoder and are trained with large-scale multimodal instruction data, enabling broad competence in captioning, visual question answering, document understanding, and multimodal reasoning [1, 2, 3, 4, 5]. This scaling trend has also improved performance on demanding benchmarks that require multi-step reasoning over images, including visual math and STEM-style problems [6, 5]. At the same time, the resulting models are increasingly expensive to deploy, motivating compression techniques that reduce latency and memory while preserving critical capabilities.

Pruning is a particularly attractive direction because it can produce hardware-friendly speedups when it removes structured components such as attention heads or whole transformer blocks. A line of work has shown that substantial redundancy exists in transformer architectures, including attention heads that can often be removed with limited impact [7, 8]. Other methods target depth directly, for example by training models that can operate at reduced depth or by selecting and removing layers after training [9, 10]. More recent efforts study post-training sparsification and structured compression for large language models, including one-shot pruning and activation-aware criteria [11, 12], as well as structural approaches that prune coupled components and recover performance via lightweight adaptation [13, 14]. Despite rapid progress, most pruning strategies are evaluated using aggregate quality metrics, leaving open a central question for multimodal deployment: which parts of a VLM are essential for a target domain, and when does the exact choice of removed layers matter?

This question is especially acute for mathematical reasoning in VLMs. Compared to generic captioning or object-centric VQA, math problems in the wild frequently require a tight coupling of perception (symbols, diagrams, tables, layout) and multi-step language reasoning. Small structural changes can therefore cause disproportionate failures, even when average vision-language scores appear stable. In language-only models, pruning has been observed to exhibit distinct regimes as sparsity increases, where mild pruning is nearly free, intermediate pruning induces transfer failures, and aggressive pruning becomes capacity-limited [15]. Whether an analogous regime structure exists for depth pruning in VLMs, and how it interacts with domain specialization, is not well understood.

In this work, we study *structured decoder layer pruning* for VLMs with the explicit goal of preserving mathematical reasoning while maintaining general vision-language competence. Our key idea is simple: a layer that barely changes its hidden representation for inputs from a particular domain is likely redundant for that domain. We operationalize this by logging the input and output activations of each decoder block on a diverse set of domain-specific probes and measuring input–output cosine similarity. This yields two complementary redundancy signals, one computed on math-oriented prompts and one computed on non-math prompts. Using these signals, we rank layers with a domain-aware criterion and prune under a fixed budget while preserving endpoint layers to avoid destabilizing early multimodal fusion and final token prediction. After pruning, we apply a brief supervised fine-tuning stage to restore stability, using the same adaptation protocol for all methods to ensure a fair comparison.

We evaluate two state-of-the-art VLMs, Qwen3-VL-2B-Instruct and Qwen3-VL-4B-Instruct [5], and report results on both math-focused benchmarks (Snapask, NuminaMath-CoT) and general-purpose benchmarks covering chart understanding, real-world spatial reasoning, multimodal science QA, and fine-grained perception [16, 17, 6, 18, 19]. Our experiments reveal a consistent *three-regime* pattern in decoder-depth pruning. At low pruning budgets, performance is highly sensitive to which layers are removed, making domain-aware ranking the most effective strategy.

At moderate budgets, methods begin to converge as structural damage accumulates. At high budgets, structural continuity becomes the limiting factor, and strategies that enforce spacing between deletions can dominate, aligning with recent structure-aware layer pruning for VLMs [20]. Across regimes, random deletion is the most brittle baseline, highlighting that redundancy in transformers is real but not uniformly distributed across depth.

Contributions.

- We introduce a domain-aware decoder layer pruning method for VLMs based on input–output activation similarity, yielding math-aware, non-math-aware, and mixed ranking variants.
- We provide an empirical regime analysis of depth pruning in VLMs, identifying ranking-sensitive, transition, and structure-dominated regimes that explain when domain-aware selection matters.
- We benchmark against representative baselines, including representation-similarity pruning and structure-aware layer pruning, and report results on both math and general vision-language evaluations.

2 Related Work

Pruning in Transformer models has been explored through head removal, structured depth reduction, and magnitude-based sparsification, demonstrating that many components contribute unevenly to model performance [7, 8, 9, 11, 12, 13, 14]. These approaches, however, are primarily developed for text-only LLMs and do not account for multimodal activation patterns.

Vision-language pruning has recently gained attention. INTERLACE introduced an interleaved prune–adapt strategy for VLMs, showing that local redundancy can be exploited effectively [20]. Other work has examined modality-specific pruning sensitivity, revealing asymmetries between visual and textual representations [21]. These methods remain modality-agnostic and do not incorporate domain-specific activation signals.

Representation similarity metrics such as CKA provide a complementary view of redundancy by identifying layers with highly aligned activation structures [21]. While CKA has been used for analysis, it has not been applied in a domain-conditioned manner for pruning. Our method differs by leveraging task-specific activation patterns to guide structured pruning tailored to mathematical reasoning.

3 Method

We study structured layer pruning for vision-language models (VLMs) with the goal of preserving mathematical reasoning while maintaining general vision-language performance. Our approach ranks transformer decoder layers by domain-specific activation similarity—measuring how much each layer transforms representations for math versus

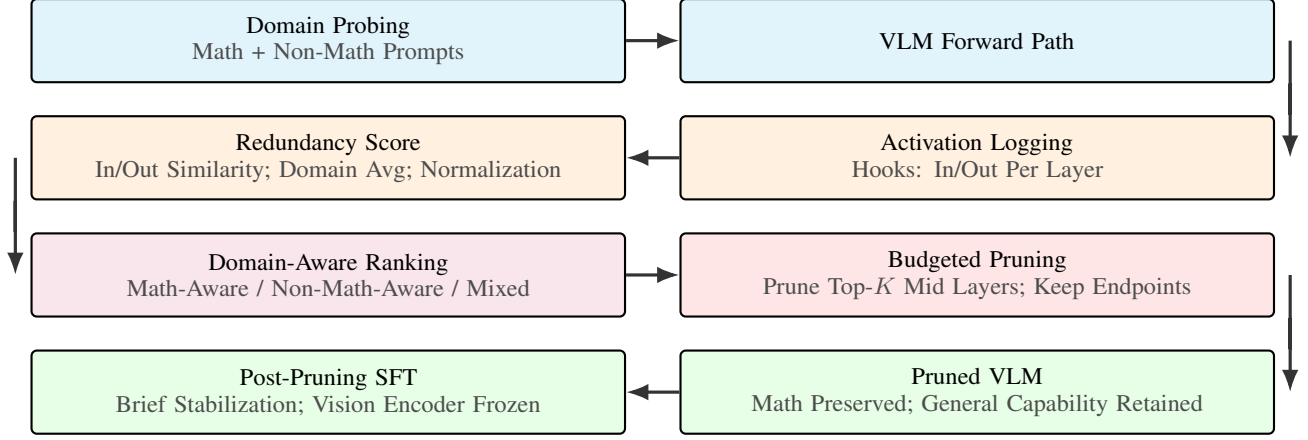


Figure 1: Overview of the domain-aware decoder layer pruning pipeline. Domain-specific prompts drive activation logging; redundancy is estimated from layer in/out similarity and aggregated per domain. Layers are ranked (math-aware, non-math-aware, or mixed) and pruned under a fixed budget with protected endpoints, and a brief SFT stabilizes the pruned model with the vision encoder kept frozen.

non-math inputs—and removes layers deemed redundant for a target domain. After pruning, we apply a lightweight post-pruning supervised fine-tuning (SFT) to recover capacity lost due to structural changes. We consider three variants of domain-aware ranking: math-aware, non-math-aware, and mixed. We then compare them against structure-agnostic and structure-aware baselines. Our method is intentionally simple, interpretable, and composable with existing pruning strategies.

3.1 Problem Setup

We consider a vision-language model based on the transformer architecture [1], following recent designs that combine a visual encoder, a projection module for cross-modal alignment, and an autoregressive language decoder [2, 3]. Given an image \mathcal{I} and a text prompt \mathcal{P} , the visual encoder produces visual tokens

$$\mathbf{Z}_v = \phi(\mathcal{I}) \in \mathbb{R}^{N_v \times d_v}, \quad (1)$$

which are projected into the language embedding space as

$$\tilde{\mathbf{Z}}_v = \psi(\mathbf{Z}_v) \in \mathbb{R}^{N_v \times d_h}. \quad (2)$$

The prompt is embedded as

$$\mathbf{Z}_t = \text{Emb}(\mathcal{P}) \in \mathbb{R}^{N_t \times d_h}, \quad (3)$$

and the decoder input is formed by concatenation:

$$\mathbf{H}^{(0)} = [\tilde{\mathbf{Z}}_v; \mathbf{Z}_t]. \quad (4)$$

The language decoder consists of L transformer layers producing hidden states

$$\mathbf{H}^{(\ell)} = \mathcal{D}_\ell(\mathbf{H}^{(\ell-1)}). \quad (5)$$

Here N_v and N_t denote the number of visual and textual tokens, d_v is the visual feature dimension, and d_h is the hidden size of the language embedding space.

We adopt depth-wise pruning, in which entire decoder layers (i.e., transformer blocks) are removed. The vision encoder and modality projection module are kept fixed, as prior studies indicate that these components are essential for maintaining stable cross-modal alignment [2, 3]. In addition, we preserve the first and last decoder layers, since they play a critical role in multimodal feature integration and final token prediction.

Let \mathcal{L}_{mid} denote the set of pruneable decoder layers. Given a pruning budget $p \in \{10\%, 25\%, 40\%\}$, we remove $K = \lfloor p \cdot |\mathcal{L}_{\text{mid}}| \rfloor$ layers.

3.2 Domain-Specific Activation Capture

Our redundancy metric is derived from the similarity between the input and output hidden representations of each decoder layer during forward inference. For every decoder layer ℓ , we capture the hidden states immediately before and after the layer via framework-level forward hooks. The input activation $H_\ell^{\text{in}} \in \mathbb{R}^{B \times T \times d}$ denotes the layer input, while the output activation $H_\ell^{\text{out}} \in \mathbb{R}^{B \times T \times d}$ denotes the corresponding layer output, where B is the batch size, T is the sequence length, and d is the hidden dimension. Each forward pass is driven by an image-prompt pair presented as a single chat message, with the image followed by text using the model’s standard template and modality tokens. For efficiency and reuse, we mean-pool activations across the batch and token dimensions to obtain per-layer vectors \bar{h}_ℓ^{in} and $\bar{h}_\ell^{\text{out}} \in \mathbb{R}^d$, which are stored in floating-point precision and reused by several baselines. Additional implementation details are provided in Appendix A.1.

3.3 Input–Output Similarity as Redundancy

For each forward pass i , we measure the degree to which a decoder layer transforms its input representation by computing the cosine similarity between its input and output hidden states at the token level:

$$\text{sim}_\ell^{(i)} = \frac{1}{T} \sum_{t=1}^T \frac{\langle h_{\ell,t}^{\text{in}}(i), h_{\ell,t}^{\text{out}}(i) \rangle}{\|h_{\ell,t}^{\text{in}}(i)\| \|h_{\ell,t}^{\text{out}}(i)\|}. \quad (6)$$

A high similarity score indicates that layer ℓ performs only a small update to the representations for that input, suggesting functional redundancy.

Domain- and subtask-specific probing. A key aspect of our method is that each domain is probed using *multiple carefully designed subtasks* rather than a single generic prompt. For the math domain, we use Math-CoT, Math-Direct, Math-Rephrase, Math-Formalize, and Math-Verify prompts; for the non-math domain, we use captioning, entity listing, counting-style VQA, and referring-expression grounding prompts. As shown in Sections A.1 and A.2, each subtask uses a distinct natural-language instruction paired with the same image.

Using diverse subtasks is essential because different prompt types trigger different computation paths inside the decoder: mathematical reasoning, linguistic paraphrasing, entity-centric grounding, and global scene understanding each activate distinct attention heads, MLP channels, and compositional behaviors. Probing with multiple prompts therefore yields a more comprehensive view of how each layer behaves across domains.

Domain-level aggregation. For each domain $d \in \{\text{math}, \text{nonmath}\}$, we aggregate the similarity scores across all subtasks and samples:

$$S_\ell^{(d)} = \frac{1}{N_d} \sum_{i=1}^{N_d} \text{sim}_\ell^{(i)}, \quad (7)$$

where the math domain uses $N_{\text{math}} = 5,000$ forward passes and the non-math domain uses $N_{\text{nonmath}} = 4,000$, distributed across their respective subtasks.

Normalization across layers. To make scores comparable across the depth of each model, we apply z-normalization within each domain:

$$\hat{S}_\ell^{(d)} = \frac{S_\ell^{(d)} - \mu_d}{\sigma_d + \epsilon}, \quad (8)$$

where μ_d and σ_d are the mean and standard deviation computed over all pruneable layers for domain d .

3.4 Layer Ranking and Pruning

Layers are ranked according to their redundancy scores and pruned in descending order under a fixed budget. We consider two domain-specific ranking strategies: a math-aware strategy using the normalized math scores $\hat{S}_\ell^{(\text{math})}$, and a non-math-aware strategy using $\hat{S}_\ell^{(\text{nonmath})}$. To combine both signals, we also construct a mixed ranking defined as

$$R_\ell(\alpha) = \alpha \hat{S}_\ell^{(\text{nonmath})} + (1 - \alpha) \hat{S}_\ell^{(\text{math})}, \quad (9)$$

where $\alpha \in [0, 1]$ controls the balance between non-math and math redundancy.

In practice, we select $\alpha = 0.7$, which we found to provide the best trade-off between maintaining general vision-language ability and preserving math reasoning performance. We intentionally give more weight to the non-math

domain because core capabilities such as OCR, VQA, and grounding are essential for stable image understanding; pruning layers that are functional for these tasks leads to significant degradation even when math reasoning layers are preserved. The value $\alpha = 0.7$ therefore provides a balanced, empirically robust ranking that retains mathematical competence without compromising baseline vision-language behavior.

3.5 Post-Pruning Stabilization

Structured pruning modifies the effective network depth and can destabilize both reasoning behavior and multimodal grounding. To restore robustness, each pruned model is subjected to a brief supervised fine-tuning (SFT) stage using a fixed mixture of mathematical and general instruction data. Applying an identical SFT protocol across all variants allows us to attribute performance differences to pruning rather than downstream adaptation.

Let the SFT dataset be $\mathcal{D}_{\text{sft}} = \{(I, x, y)\}$, where I denotes the input image, x the textual instruction, and y the target response. We optimize the standard maximum-likelihood objective

$$\mathcal{L}_{\text{SFT}}(\theta) = -\mathbb{E}_{(I,x,y) \sim \mathcal{D}_{\text{sft}}} [\log p_{\theta}(y | I, x)], \quad (10)$$

where p_{θ} is the conditional output distribution of the pruned model. This objective encourages accurate instruction following conditioned on both visual and textual inputs, and empirically mitigates performance degradation introduced by structural pruning.

4 Experiments and Dataset

4.1 Dataset

Our experiments draw on a mixture of proprietary and public multimodal datasets that collectively cover real-world homework photos, general vision-language tasks, scientific diagrams, chart reasoning, and fine-grained visual perception. Below we summarize each dataset, its size, and its role in training or evaluation.

Snapask. Snapask is a proprietary collection of roughly 300,000 real-world homework photographs spanning algebra, geometry, and general mathematics. Each image includes a curated GPT-4o [22] chain-of-thought solution. Following our internal data protocol, we use 100,000 examples for training and reserve a held-out evaluation set of 2,540 questions. Snapask provides the primary source of mathematical supervision for instruction tuning.

LLaVA-OneVision. LLaVA-OneVision contains 105,000 multimodal instruction-following samples covering charts, scientific figures, compositional reasoning, scene description, and VQA. We adopt the official 100k training split and the 5k held-out test split. This dataset supplies broad general-purpose vision-language coverage complementary to Snapask [23, 4, 24].

NuminaMath-CoT. NuminaMath-CoT [25] consists of high-difficulty mathematical problems, including Olympiad-style and competition-level items paired with chain-of-thought solutions. To assess robustness under domain shift, we evaluate on a curated set of 500 items. Following [26], all problems originally provided in text form are rendered as images.

ChartQA. ChartQA [16] evaluates chart and data visualization reasoning. It contains 9.6k human-authored questions and 23.1k automatically generated questions spanning bar charts, line plots, and statistical graphics. We use the standard 2,500-sample test split.

ScienceQA. ScienceQA [6] includes 21,208 multimodal science questions spanning biology, physics, earth science, and general STEM topics. Many questions contain diagrams or textbook-style illustrations. We use the official 2,017-example evaluation split.

RealWorldQA. RealWorldQA [17] provides 765 real-world images paired with spatial or geometric reasoning questions. We evaluate on the full test set to measure robustness in real-world spatial understanding.

VStar. VStar [18] is a fine-grained visual perception benchmark containing 191 tasks designed to evaluate subtle spatial relations, small-target identification, and fine-detail recognition in cluttered, high-resolution scenes.

Dataset	Size	Purpose
Snapask	300K total (100K train; 2,540 eval)	Real-world homework photos with CoT solutions; primary math supervision.
LLaVA-OneVision	105K total (100K train; 5K eval)	Broad multimodal instruction tuning: charts, diagrams, scenes, VQA.
NuminaMath-CoT	500 eval samples	High-difficulty math reasoning; domain-shift robustness.
ChartQA	32.7K questions (2,500 eval)	Reasoning over charts and structured data visualizations.
ScienceQA	21,208 total (2,017 eval)	Multimodal science questions with diagrams and multi-step reasoning.
RealWorldQA	765 images (full eval)	Real-world spatial and geometric reasoning.
VStar	191 tasks	Fine-grained visual perception and small-target identification.

Table 1: Training and evaluation datasets used in our experiments. Activation-analysis data is documented separately in Appendix A.1.

4.2 Training and Implementation Details

All experiments are conducted using the Qwen3-VL-2B-Instruct and Qwen3-VL-4B-Instruct models. Structured pruning is applied exclusively to decoder layers, while the first and last decoder layers remain fixed. We evaluate three pruning budgets, 10%, 25%, and 40%, measured as the proportion of pruneable decoder layers removed. To ensure a fair comparison, both baseline and pruned models share identical LoRA [27] configurations as well as identical optimization hyperparameters.

Training and evaluation are performed on 8 NVIDIA V100 GPUs (32 GB each). The training mixture consists of 100k sampled Snapask examples combined with 100k instances from the LLaVA-OneVision training split, following the preprocessing pipeline described in Section 4.1. For held-out evaluation, we use the 5,000-sample LLaVA-OneVision test set, the Snapask validation subset (2,540 samples), and the competition-level NuminaMath-CoT benchmark.

We perform supervised fine-tuning (SFT) on the constructed training set using DeepSpeed ZeRO-3 [28, 29, 30] to improve memory efficiency and scalability. Optimization follows a cosine learning-rate schedule with an initial learning rate of 2×10^{-5} , an effective batch size of 64, a single training epoch, weight decay of 0.1, and a maximum sequence length of 8,192 tokens. Parameter-efficient adaptation is implemented via LoRA [27] with rank $r = 32$, $\alpha = 64$, and dropout rate 0.05.

For broader multimodal evaluation, we additionally report results using the `lmms-eval` framework [19] on the following benchmarks:

- ChartQA [16]
- RealWorldQA [17]
- ScienceQA [6]
- VStar [18]

To compute accuracy on LLaVA-OneVision, Snapask, and NuminaMath-CoT, we use GPT-5 [31] to compare the model’s predicted responses against the ground-truth answers.

4.3 Baseline Pruning Methods

To contextualize the effectiveness of our domain-aware pruning strategy, we compare against three widely used baselines representing complementary pruning philosophies: representation-similarity pruning, structure-aware pruning, and uninformed random removal.

CKA-based pruning. We employ *linear Centered Kernel Alignment (CKA)* [21] to quantify how similarly two consecutive decoder layers represent their inputs. CKA is a representation-similarity metric that is invariant to isotropic scaling and orthogonal transformations, making it robust to the natural feature rotations that occur in deep networks [21]. In our setting, for each layer ℓ , we construct a feature matrix $X_\ell \in \mathbb{R}^{9 \times d}$ by stacking the mean-pooled activation vectors from the nine probing tasks (five math tasks and four non-math tasks), treating each task as a pseudo-sample. After

centering the features, we compute linear CKA between layers ℓ and $\ell+1$ as

$$\text{CKA}(X_\ell, X_{\ell+1}) = \frac{\left\| \tilde{X}_\ell^\top \tilde{X}_{\ell+1} \right\|_F^2}{\left\| \tilde{X}_\ell^\top \tilde{X}_\ell \right\|_F \left\| \tilde{X}_{\ell+1}^\top \tilde{X}_{\ell+1} \right\|_F}.$$

A high CKA value indicates that the two layers encode highly aligned information and thus perform similar transformations on the probing tasks [21]. We therefore interpret high $\text{CKA}(\ell, \ell+1)$ as evidence that layer $\ell+1$ is *redundant* given layer ℓ . Layers are ranked by redundancy and pruned from highest to lowest under the same budget and protection rules described in Section 3.4.

Interlace pruning. Interlace [20] is a structure-aware depth pruning strategy designed to avoid the instability caused by removing many adjacent layers, a common failure mode of similarity-only methods. Interlace analyzes *local triplets* of layers $(\ell, \ell+1, \ell+2)$, using the same nine pseudo-sample activations as in our CKA baseline. For each layer, we first compute a cosine similarity

$$S_\ell = \frac{1}{9} \sum_{i=1}^9 \cos\left(h_\ell^{(i)}, h_{\ell+1}^{(i)}\right),$$

where $h_\ell^{(i)}$ is the mean-pooled activation for task i . Each triplet receives a *triplet redundancy score*

$$R_{(\ell, \ell+1, \ell+2)} = \frac{S_\ell + S_{\ell+1}}{2},$$

which captures how weakly the layers in that local region transform their representations [20]. Triplets are then sorted by R and selected greedily under a strict *non-overlap constraint*, ensuring that no two chosen triplets touch. Within each selected triplet, Interlace removes exactly one layer—the more redundant of ℓ or $\ell+1$ —while always preserving $\ell+2$ as a stable *anchor layer*. This explicit spacing constraint prevents the formation of long contiguous holes in the network, making Interlace particularly effective at higher pruning budgets where structural collapse otherwise becomes a limiting factor [20].

Random pruning. Random pruning selects K pruneable layers uniformly at random (seeded for reproducibility). Despite its simplicity, prior work has shown that random removal can be surprisingly competitive in large models, making it a necessary sanity-check baseline.

All baselines are followed by the same post-pruning SFT procedure described in Section 3.5, ensuring that differences in performance stem solely from the pruning strategy rather than subsequent adaptation.

5 Results

We report accuracy across math benchmarks (Snapask, NuminaMath) and general vision-language benchmarks (LLaVA-OneVision, ChartQA, RealWorldQA, ScienceQA, VStar). All deltas are computed relative to the *unpruned baseline model without fine-tuning*. Appendix Table 6 reports the corresponding baseline+SFT values.

Cell format. Each table cell is reported as

$$\text{Acc}(\Delta_{\text{abs}}, \Delta_{\text{rel}}), \quad \Delta_{\text{abs}} = \text{Acc} - \text{Acc}_{\text{Baseline}}, \quad \Delta_{\text{rel}} = 100 \cdot \frac{\Delta_{\text{abs}}}{\text{Acc}_{\text{Baseline}}}.$$

Bold indicates the highest accuracy among pruned variants at that budget.

High-level trends. Figure 2 visualizes the three pruning regimes underlying our results. At low budgets, which layers are removed matters most; at high budgets the model becomes structure-limited. These regimes are visible across both model scales and both domains.

5.1 Math domain: Snapask and NuminaMath

Snapask consists of real-world homework photos, where problems are often accompanied by diagrams, tables, and other visual elements. NuminaMath contains competition-style math problems that exhibit significant domain shift. Across both benchmarks, we observe a clear regime structure: domain-aware ranking is most effective under low-budget settings, whereas structural constraints become dominant at higher budgets.

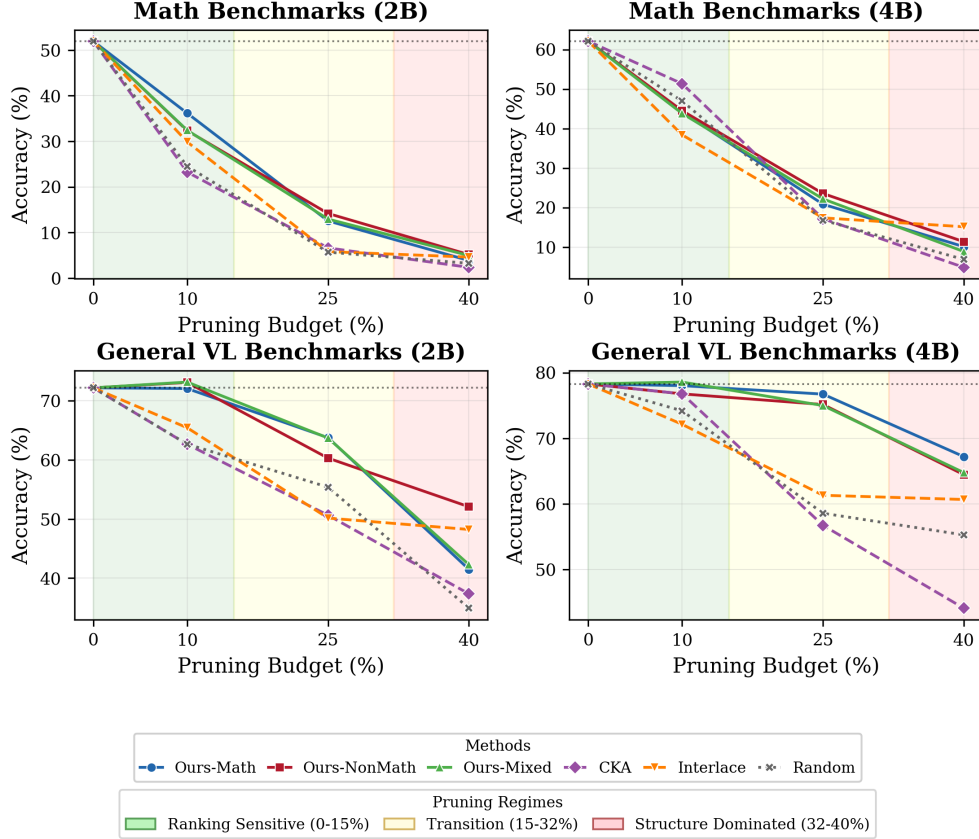


Figure 2: Accuracy versus pruning budget across domains and model sizes. Shaded regions highlight the ranking-sensitive regime (0–15%), transition regime (15–32%), and structure-dominated regime (32–40%). Domain-aware methods separate most strongly at low budgets, while structural continuity becomes limiting at high budgets.

Table 2: Math results for Qwen3-VL-2B. Deltas are relative to the unpruned baseline without fine-tuning.

Budget 10% (ranking-sensitive regime)						
Dataset	Ours-Math	Ours-NonMath	Ours-Mixed	CKA	Interlace	Random
Snapask	28.15 (-12.32, -30.4%)	24.69 (-15.78, -39.0%)	24.88 (-15.59, -38.5%)	15.98 (-24.49, -60.5%)	20.75 (-19.72, -48.7%)	17.09 (-23.38, -57.8%)
NuminaMath	44.18 (-19.27, -30.4%)	39.96 (-23.49, -37.0%)	39.96 (-23.49, -37.0%)	30.52 (-32.93, -51.9%)	38.96 (-24.49, -38.6%)	31.93 (-31.52, -49.7%)
Budget 25% (transition regime)						
Dataset	Ours-Math	Ours-NonMath	Ours-Mixed	CKA	Interlace	Random
Snapask	9.21 (-31.26, -77.2%)	11.06 (-29.41, -72.7%)	9.61 (-30.86, -76.3%)	4.80 (-35.67, -88.1%)	5.17 (-35.30, -87.2%)	4.72 (-35.75, -88.3%)
NuminaMath	15.86 (-47.59, -75.0%)	17.27 (-46.18, -72.8%)	16.27 (-47.18, -74.4%)	8.43 (-55.02, -86.7%)	6.43 (-57.02, -89.9%)	6.63 (-56.82, -89.6%)
Budget 40% (structure-dominated regime)						
Dataset	Ours-Math	Ours-NonMath	Ours-Mixed	CKA	Interlace	Random
Snapask	3.46 (-37.01, -91.5%)	4.06 (-36.41, -90.0%)	4.65 (-35.82, -88.5%)	2.48 (-37.99, -93.9%)	4.57 (-35.90, -88.7%)	2.44 (-38.03, -94.0%)
NuminaMath	4.22 (-59.23, -93.3%)	6.22 (-57.23, -90.2%)	5.22 (-58.23, -91.8%)	2.21 (-61.24, -96.5%)	4.62 (-58.83, -92.7%)	4.02 (-59.43, -93.7%)

Math insights across regimes. For the 2B model at 10%, domain-aware ranking is consistently the most stable. At higher budgets, all methods deteriorate sharply, reflecting the depth sensitivity of math reasoning. For the 4B model, 10% remains competitive, but at 40%, Interlace becomes the most stable due to its spaced layer deletions, which avoid contiguous holes that disrupt long-range residual flow.

Appendix Figures 6, 7, and 8 provide a compact view of relative degradation and per-benchmark curves.

Math-General VL trade-off. To summarize how pruning affects mathematical reasoning and general multimodal ability jointly, Figure 3 plots Math accuracy against General VL accuracy for all methods and pruning budgets. Each point corresponds to a (method, budget) pair, with marker size indicating pruning budget. The unpruned baseline

Table 3: Math results for Qwen3-VL-4B. Deltas are relative to the unpruned baseline without fine-tuning.

Budget 10% (ranking-sensitive regime)						
Dataset	Ours-Math	Ours-NonMath	Ours-Mixed	CKA	Interlace	Random
Snapask	35.83 (-14.92, -29.4%)	33.54 (-17.21, -33.9%)	33.23 (-17.52, -34.5%)	40.24 (-10.51, -20.7%)	28.82 (-21.93, -43.2%)	37.09 (-13.66, -26.9%)
NuminaMath	52.41 (-21.08, -28.7%)	55.50 (-17.99, -24.5%)	54.42 (-19.07, -25.9%)	62.45 (-11.04, -15.0%)	47.99 (-25.50, -34.7%)	56.83 (-16.66, -22.7%)
Budget 25% (transition regime)						
Dataset	Ours-Math	Ours-NonMath	Ours-Mixed	CKA	Interlace	Random
Snapask	15.98 (-34.77, -68.5%)	18.19 (-32.56, -64.2%)	16.26 (-34.49, -68.0%)	12.44 (-38.31, -75.5%)	12.09 (-38.66, -76.2%)	11.30 (-39.45, -77.7%)
NuminaMath	25.70 (-47.79, -65.0%)	28.92 (-44.57, -60.6%)	28.11 (-45.38, -61.7%)	21.89 (-51.60, -70.2%)	22.69 (-50.80, -69.1%)	22.29 (-51.20, -69.7%)
Budget 40% (structure-dominated regime)						
Dataset	Ours-Math	Ours-NonMath	Ours-Mixed	CKA	Interlace	Random
Snapask	9.76 (-40.99, -80.8%)	9.06 (-41.69, -82.1%)	7.68 (-43.07, -84.9%)	3.70 (-47.05, -92.7%)	10.79 (-39.96, -78.7%)	5.51 (-45.24, -89.1%)
NuminaMath	10.44 (-63.05, -85.8%)	13.65 (-59.84, -81.4%)	10.04 (-63.45, -86.3%)	6.02 (-67.47, -91.8%)	19.48 (-54.01, -73.5%)	8.23 (-65.26, -88.8%)

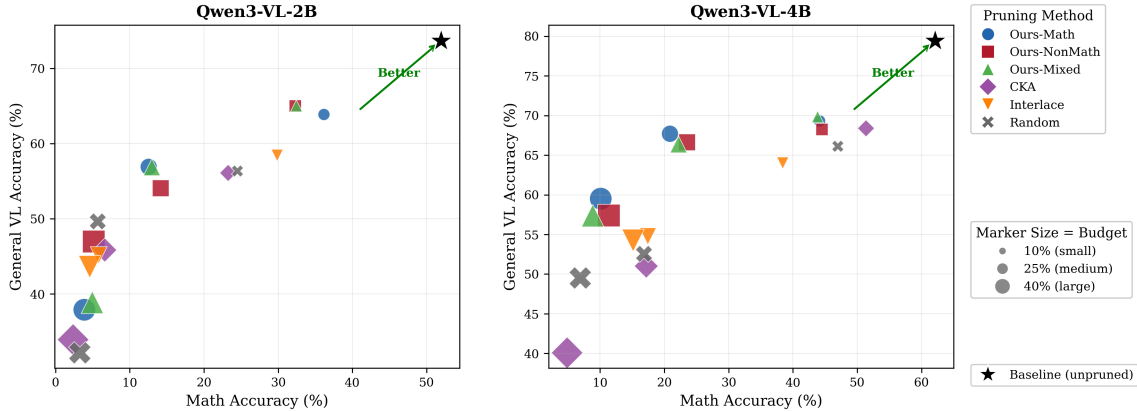


Figure 3: Trade-off between Math accuracy (x-axis) and General Vision-Language accuracy (y-axis) for Qwen3-VL-2B (left) and Qwen3-VL-4B (right). Each point represents a pruning method at a given budget; marker size increases with pruning budget (10%, 25%, 40%). The black star denotes the unpruned baseline. Domain-aware methods (circles) lie on or near the Pareto frontier, achieving the best balance between math and general VL performance. CKA and Random pruning are consistently dominated, while Interlace maintains general VL stability but exhibits steeper math degradation at higher budgets.

appears in the upper-right corner. Domain-aware methods trace a Pareto-efficient frontier: Ours-Math shifts rightward (stronger math retention), Ours-NonMath shifts upward (stronger general VL retention), and Ours-Mixed consistently lies near the diagonal frontier, offering the best balance. In contrast, CKA and Random pruning are dominated across both axes, while Interlace maintains reasonable general VL performance but suffers sharper math degradation at higher budgets. This trade-off view highlights that domain-aware ranking provides the most favorable balance when both math and general multimodal capability must be preserved.

5.2 General vision-language: LLaVA-OneVision, ChartQA, RealWorldQA, ScienceQA, VStar

We evaluate general vision-language ability using LLaVA-OneVision and four lms-eva1 benchmarks [19], each targeting different skills: ChartQA (structured chart parsing), RealWorldQA (spatial grounding), ScienceQA (diagram reasoning), and VStar (fine-grained perception). The transition from ranking sensitivity to structure sensitivity is visible across all tasks as the pruning budget increases.

Task-level insights beyond averages. ChartQA. ChartQA is consistently fragile under our fixed post-pruning SFT mixture, producing large absolute drops relative to the no-SFT baseline across all pruning strategies and budgets. Appendix Table 6 shows that the unpruned baseline+SFT itself is much lower than the baseline on ChartQA, indicating that the primary driver is the distribution shift induced by the stabilization SFT rather than the specific pruning strategy. Under this constraint, mixed and non-math rankings are still the most stable among pruned models at each budget, suggesting that preserving general vision-language layers is preferable when chart-specific data is not present in the SFT mixture.

Table 4: General vision-language results for Qwen3-VL-2B. Deltas are relative to the unpruned baseline without fine-tuning. Scores for ChartQA, RealWorldQA, ScienceQA, and VStar are obtained using `lmms-eval` [19].

Budget 10% (ranking-sensitive regime)						
Dataset	Ours-Math	Ours-NonMath	Ours-Mixed	CKA	Interlace	Random
LLaVA-OneVision	60.74 (+1.62, +2.7%)	60.76 (+1.64, +2.8%)	60.76 (+1.64, +2.8%)	53.84 (-5.28, -8.9%)	57.70 (-1.42, -2.4%)	54.38 (-4.74, -8.0%)
ChartQA	31.28 (-48.44, -60.8%)	32.68 (-47.04, -59.0%)	32.60 (-47.12, -59.1%)	30.08 (-49.64, -62.3%)	30.60 (-49.12, -61.6%)	31.16 (-48.56, -60.9%)
RealWorldQA	65.10 (-0.13, -0.2%)	67.45 (+2.22, +3.4%)	67.32 (+2.09, +3.2%)	59.87 (-5.36, -8.2%)	61.70 (-3.53, -5.4%)	61.44 (-3.79, -5.8%)
ScienceQA	88.15 (+1.68, +1.9%)	87.31 (+0.84, +1.0%)	87.70 (+1.23, +1.4%)	74.07 (-12.40, -14.3%)	73.82 (-12.65, -14.6%)	70.50 (-15.97, -18.5%)
VStar	74.35 (-3.66, -4.7%)	76.96 (-1.05, -1.3%)	76.96 (-1.05, -1.3%)	62.83 (-15.18, -19.5%)	68.59 (-9.42, -12.1%)	64.40 (-13.61, -17.4%)
Budget 25% (transition regime)						
Dataset	Ours-Math	Ours-NonMath	Ours-Mixed	CKA	Interlace	Random
LLaVA-OneVision	50.62 (-8.50, -14.4%)	50.52 (-8.60, -14.5%)	50.56 (-8.56, -14.5%)	43.70 (-15.42, -26.1%)	42.47 (-16.65, -28.2%)	46.80 (-12.32, -20.8%)
ChartQA	29.56 (-50.16, -62.9%)	29.04 (-50.68, -63.6%)	29.64 (-50.08, -62.8%)	26.68 (-53.04, -66.5%)	25.24 (-54.48, -68.3%)	26.80 (-52.92, -66.4%)
RealWorldQA	58.95 (-6.28, -9.6%)	58.43 (-6.80, -10.4%)	58.95 (-6.28, -9.6%)	50.20 (-15.03, -23.0%)	47.84 (-17.39, -26.7%)	55.29 (-9.94, -15.2%)
ScienceQA	75.90 (-10.57, -12.2%)	68.42 (-18.05, -20.9%)	75.71 (-10.76, -12.4%)	58.95 (-27.52, -31.8%)	59.54 (-26.93, -31.1%)	61.38 (-25.09, -29.0%)
VStar	69.63 (-8.38, -10.7%)	63.87 (-14.14, -18.1%)	69.63 (-8.38, -10.7%)	49.74 (-28.27, -36.2%)	50.79 (-27.22, -34.9%)	58.12 (-19.89, -25.5%)
Budget 40% (structure-dominated regime)						
Dataset	Ours-Math	Ours-NonMath	Ours-Mixed	CKA	Interlace	Random
LLaVA-OneVision	37.32 (-21.80, -36.9%)	43.22 (-15.90, -26.9%)	40.38 (-18.74, -31.7%)	34.58 (-24.54, -41.5%)	40.94 (-18.18, -30.8%)	32.64 (-26.48, -44.8%)
ChartQA	23.72 (-56.00, -70.2%)	26.56 (-53.16, -66.7%)	25.52 (-54.20, -68.0%)	20.40 (-59.32, -74.4%)	25.36 (-54.36, -68.2%)	21.48 (-58.24, -73.1%)
RealWorldQA	45.88 (-19.35, -29.7%)	52.81 (-12.42, -19.0%)	47.19 (-18.04, -27.7%)	40.26 (-24.97, -38.3%)	48.24 (-16.99, -26.0%)	36.73 (-28.50, -43.7%)
ScienceQA	42.94 (-43.53, -50.3%)	57.31 (-29.16, -33.7%)	44.37 (-42.10, -48.7%)	35.25 (-51.22, -59.2%)	57.16 (-29.31, -33.9%)	35.15 (-51.32, -59.4%)
VStar	39.79 (-38.22, -49.0%)	54.97 (-23.04, -29.5%)	37.17 (-40.84, -52.4%)	39.27 (-38.74, -49.7%)	46.60 (-31.41, -40.3%)	35.08 (-42.93, -55.0%)

Table 5: General vision-language results for Qwen3-VL-4B. Deltas are relative to the unpruned baseline without fine-tuning. Scores for ChartQA, RealWorldQA, ScienceQA, and VStar are obtained using `lmms-eval` [19].

Budget 10% (ranking-sensitive regime)						
Dataset	Ours-Math	Ours-NonMath	Ours-Mixed	CKA	Interlace	Random
LLaVA-OneVision	66.16 (-1.10, -1.6%)	64.62 (-2.64, -3.9%)	66.02 (-1.24, -1.8%)	66.82 (-0.44, -0.7%)	63.14 (-4.12, -6.1%)	64.56 (-2.70, -4.0%)
ChartQA	34.48 (-49.52, -59.0%)	34.12 (-49.88, -59.4%)	35.04 (-48.96, -58.3%)	34.84 (-49.16, -58.5%)	31.56 (-52.44, -62.4%)	33.84 (-50.16, -59.7%)
RealWorldQA	71.63 (+0.13, +0.2%)	69.54 (-1.96, -2.7%)	72.29 (+0.79, +1.1%)	71.11 (-0.39, -0.5%)	64.97 (-6.53, -9.1%)	67.97 (-3.53, -4.9%)
ScienceQA	93.16 (+0.45, +0.5%)	91.77 (-0.94, -1.0%)	93.26 (+0.55, +0.6%)	86.47 (-6.24, -6.7%)	86.61 (-6.10, -6.6%)	86.22 (-6.49, -7.0%)
VStar	81.15 (-0.53, -0.6%)	81.15 (-0.53, -0.6%)	82.72 (+1.04, +1.3%)	82.72 (+1.04, +1.3%)	73.82 (-7.86, -9.6%)	78.01 (-3.67, -4.5%)
Budget 25% (transition regime)						
Dataset	Ours-Math	Ours-NonMath	Ours-Mixed	CKA	Interlace	Random
LLaVA-OneVision	61.78 (-5.48, -8.1%)	61.32 (-5.94, -8.8%)	60.78 (-6.48, -9.6%)	51.86 (-15.40, -22.9%)	55.20 (-12.06, -17.9%)	51.76 (-15.50, -23.0%)
ChartQA	31.60 (-52.40, -62.4%)	32.40 (-51.60, -61.4%)	32.00 (-52.00, -61.9%)	28.24 (-55.76, -66.4%)	28.64 (-55.36, -65.9%)	28.60 (-55.40, -66.0%)
RealWorldQA	70.46 (-1.04, -1.5%)	68.76 (-2.74, -3.8%)	68.50 (-3.00, -4.2%)	57.91 (-13.59, -19.0%)	62.88 (-8.62, -12.1%)	58.43 (-13.07, -18.3%)
ScienceQA	91.97 (-0.74, -0.8%)	90.43 (-2.28, -2.5%)	91.62 (-1.09, -1.2%)	61.68 (-31.03, -33.5%)	68.02 (-24.69, -26.6%)	66.53 (-26.18, -28.2%)
VStar	82.72 (+1.04, +1.3%)	80.10 (-1.58, -1.9%)	79.06 (-2.62, -3.2%)	55.50 (-26.18, -32.1%)	59.16 (-22.52, -27.6%)	57.59 (-24.09, -29.5%)
Budget 40% (structure-dominated regime)						
Dataset	Ours-Math	Ours-NonMath	Ours-Mixed	CKA	Interlace	Random
LLaVA-OneVision	53.88 (-13.38, -19.9%)	54.00 (-13.26, -19.7%)	50.72 (-16.54, -24.6%)	40.72 (-26.54, -39.5%)	54.26 (-13.00, -19.3%)	46.64 (-20.62, -30.7%)
ChartQA	28.92 (-55.08, -65.6%)	29.04 (-54.96, -65.4%)	27.96 (-56.04, -66.7%)	24.20 (-59.80, -71.2%)	28.64 (-55.36, -65.9%)	26.64 (-57.36, -68.3%)
RealWorldQA	63.01 (-8.49, -11.9%)	61.70 (-9.80, -13.7%)	60.92 (-10.58, -14.8%)	46.27 (-25.23, -35.3%)	62.88 (-8.62, -12.1%)	56.73 (-14.77, -20.7%)
ScienceQA	81.76 (-10.95, -11.8%)	73.53 (-19.18, -20.7%)	79.38 (-13.33, -14.4%)	50.67 (-42.04, -45.3%)	67.97 (-24.74, -26.7%)	64.85 (-27.86, -30.1%)
VStar	70.16 (-11.52, -14.1%)	68.59 (-13.09, -16.0%)	68.06 (-13.62, -16.7%)	38.74 (-42.94, -52.6%)	57.59 (-24.09, -29.5%)	52.88 (-28.80, -35.3%)

RealWorldQA. RealWorldQA remains close to baseline at 10% for both scales, with mixed or non-math ranking performing best. At higher budgets, the most stable outcomes shift toward strategies that avoid removing early-to-mid layers, consistent with RealWorldQA requiring robust spatial grounding and cross-modal alignment. This aligns with the fact that our math-aware pruning tends to target later layers, while CKA removes earlier blocks more aggressively.

ScienceQA. ScienceQA behaves more like a reasoning benchmark than a pure perception benchmark: at 10% the best methods often match or slightly exceed the baseline, and at 25% the math-aware variant is consistently strongest for both 2B and 4B. This is consistent with ScienceQA requiring multi-step language reasoning conditioned on diagrams, benefiting from preserving reasoning-critical mid-depth computation while pruning redundant late layers. The layer logs confirm that math-aware pruning concentrates deletions in late layers for both model sizes at small budgets.

VStar. VStar is sensitive to aggressive pruning but can tolerate mild pruning. At 10%, mixed and CKA reach the best scores in 4B, while non-math and mixed are most stable in 2B. This suggests that fine-grained perception benefits from preserving early and mid layers and that removing redundant late layers can be safe, but once pruning becomes aggressive the task becomes structure-limited.

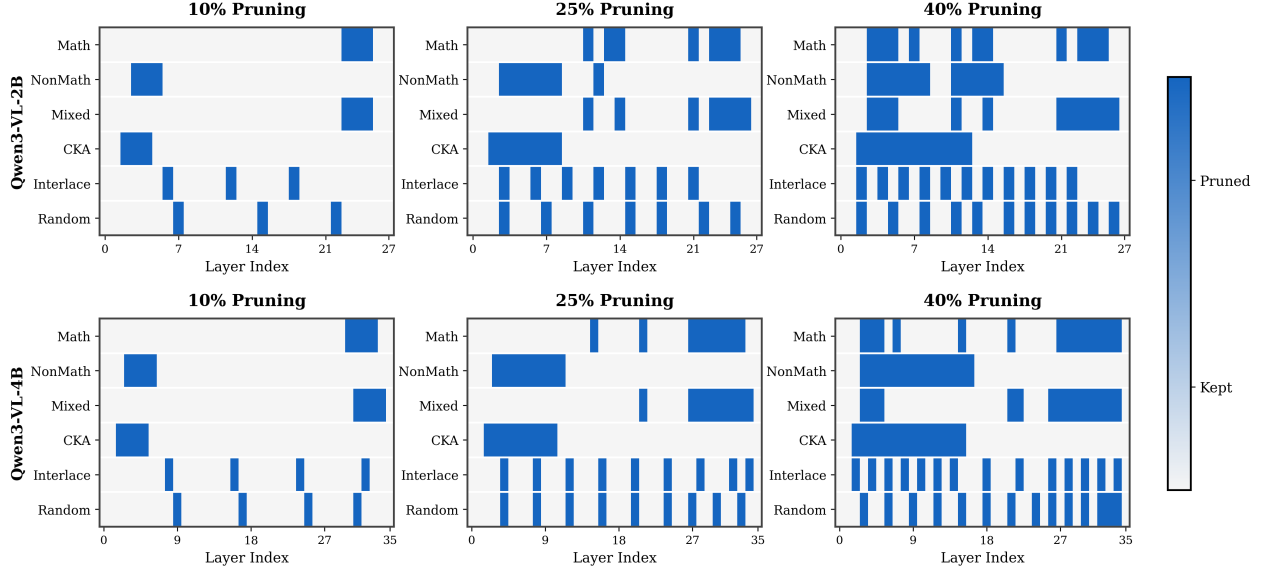


Figure 4: Decoder layer removal patterns across methods, budgets, and model sizes. Dark cells indicate pruned layers; light cells indicate retained layers. Domain-aware methods produce structured patterns, while Interlace enforces spaced deletions and Random remains unstructured.

Appendix Figures 7–8 show full per-benchmark curves.

5.3 Layer removal patterns and regime transitions

To understand why pruning strategies behave differently across budgets, we first examine how strongly each decoder layer transforms its representations under the probing tasks used to compute redundancy scores. Figure 5 visualizes the input–output cosine similarity for every layer across all math and non-math subtasks. Layers with higher similarity perform weaker updates and are therefore more pruneable under our criterion. The heatmaps reveal a consistent structure across both model sizes: math subtasks elicit stronger activations in mid–late layers, while non-math subtasks rely more on early–mid layers. These domain-specific activation patterns directly shape the behavior of our math-aware, non-math-aware, and mixed rankings.

Figure 4 shows the exact pruned layers for each method, budget, and model scale. The mid-depth deletions vary significantly across strategies.

Math-aware ranking concentrates deletions in the later layers at small budgets, while non-math-aware and mixed rankings begin removing earlier blocks as the budget grows. CKA consistently targets early layers, whereas Interlace enforces evenly spaced deletions across depth.

These patterns explain the regimes in Figure 2. At low budgets, ranking is most effective because it avoids deleting critical computation. At high budgets, the model becomes structure-limited, and strategies that preserve continuity—especially Interlace—become more stable.

Random pruning produces the largest drops across domains because it deletes early or mid-depth blocks without structural safeguards, often producing irregular gaps.

References

- [1] Ashish Vaswani, Noam Shazeer, Niki Parmar, Jakob Uszkoreit, Llion Jones, Aidan N. Gomez, Łukasz Kaiser, and Illia Polosukhin. Attention is all you need. In *Advances in Neural Information Processing Systems (NeurIPS)*, 2017.
- [2] Junnan Li, Dongxu Li, Silvio Savarese, and Steven Hoi. BLIP-2: Bootstrapping language-image pre-training with frozen image encoders and large language models. In *Proceedings of the 40th International Conference on Machine Learning (ICML)*, volume 202 of *Proceedings of Machine Learning Research*, pages 19730–19742, 2023.

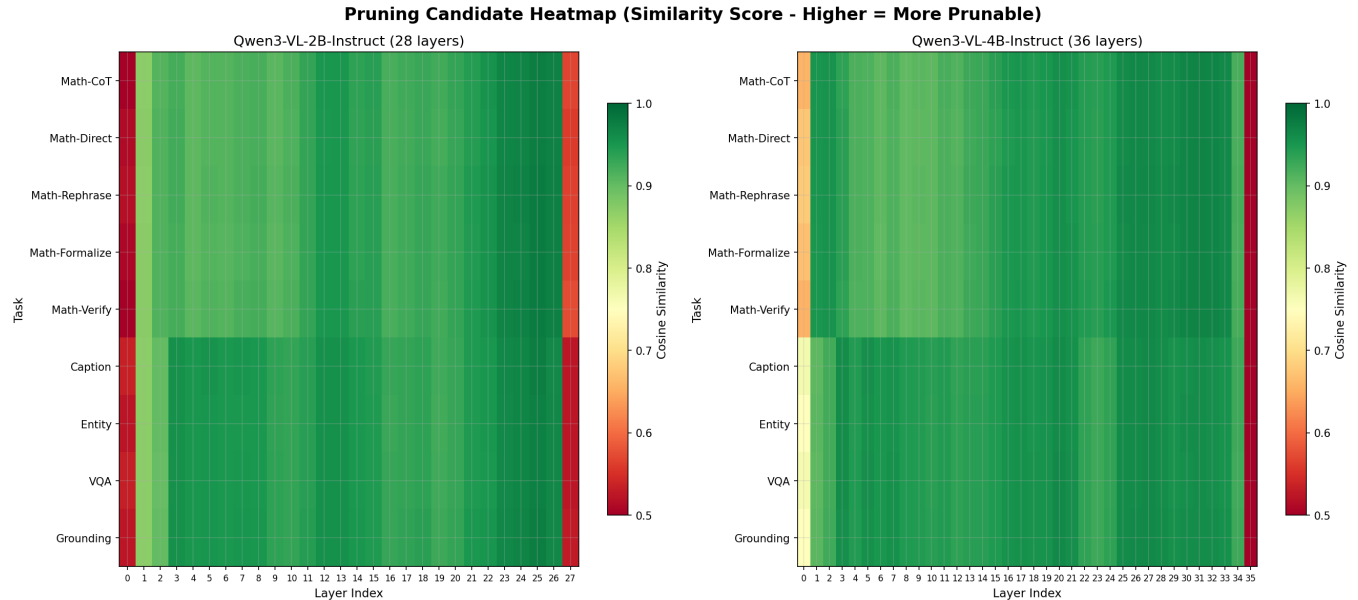


Figure 5: Pruning candidate heatmaps for Qwen3-VL-2B (left) and Qwen3-VL-4B (right). Each cell shows the cosine similarity between a layer’s input and output activations for a given probing subtask. Higher similarity indicates weaker transformation and thus higher pruneability. Math subtasks (top rows) and non-math subtasks (bottom rows) exhibit distinct activation patterns, motivating domain-aware layer ranking.

- [3] Haotian Liu, Chunyuan Li, Qingyang Wu, and Yong Jae Lee. Visual instruction tuning. In *Advances in Neural Information Processing Systems (NeurIPS)*, 2023.
- [4] Bo Li, Yuanhan Zhang, Dong Guo, Renrui Zhang, Feng Li, Hao Zhang, Kaichen Zhang, Peiyuan Zhang, Yanwei Li, Ziwei Liu, and Chunyuan Li. Llava-onevision: Easy visual task transfer, 2024.
- [5] Shuai Bai, Yuxuan Cai, Ruizhe Chen, Keqin Chen, Xionghui Chen, Zesen Cheng, Lianghao Deng, Wei Ding, Chang Gao, Chunjiang Ge, et al. Qwen3-vl technical report, 2025.
- [6] Pan Lu, Swaroop Mishra, Tony Xia, Liang Qiu, Kai-Wei Chang, Song-Chun Zhu, Oyvind Tafjord, Peter Clark, and Ashwin Kalyan. Learn to explain: Multimodal reasoning via thought chains for science question answering. In *Advances in Neural Information Processing Systems (NeurIPS)*, 2022.
- [7] Paul Michel, Omer Levy, and Graham Neubig. Are sixteen heads really better than one? In *Advances in Neural Information Processing Systems (NeurIPS)*, 2019.
- [8] Elena Voita, David Talbot, Fedor Moiseev, Rico Sennrich, and Ivan Titov. Analyzing multi-head self-attention: Specialized heads do the heavy lifting, the rest can be pruned. In *Proceedings of the 57th Annual Meeting of the Association for Computational Linguistics (ACL)*, pages 5797–5808, 2019.
- [9] Angela Fan, Edouard Grave, and Armand Joulin. Reducing transformer depth on demand with structured dropout, 2019.
- [10] David Peer, Sebastian Stabinger, Stefan Engl, and Antonio Rodriguez-Sanchez. Greedy-layer pruning: Speeding up transformer models for natural language processing, 2022.
- [11] Elias Frantar and Dan Alistarh. SparseGPT: Massive language models can be accurately pruned in one-shot. In *Proceedings of the 40th International Conference on Machine Learning (ICML)*, volume 202 of *Proceedings of Machine Learning Research*, pages 10323–10337, 2023.
- [12] Mingjie Sun, Zhuang Liu, Anna Bair, and J. Zico Kolter. A simple and effective pruning approach for large language models. In *International Conference on Learning Representations (ICLR)*, 2024.
- [13] Xinyin Ma, Gongfan Fang, and Xinchao Wang. Llm-pruner: On the structural pruning of large language models. In *Advances in Neural Information Processing Systems (NeurIPS)*, 2023.
- [14] Saleh Ashkboos, Maximilian L. Croci, Marcelo Gennari do Nascimento, Torsten Hoefler, and James Hensman. Slicept: Compress large language models by deleting rows and columns. In *International Conference on Learning Representations (ICLR)*, 2024.

- [15] Mitchell A. Gordon, Kevin Duh, and Nicholas Andrews. Compressing bert: Studying the effects of weight pruning on transfer learning. In *Proceedings of the 4th Workshop on Representation Learning for NLP (RepL4NLP)*, 2020.
- [16] Ahmed Masry, Do Xuan Long, Jia Qing Tan, Shafiq Joty, and Enamul Hoque. Chartqa: A benchmark for question answering about charts with visual and logical reasoning. In *Findings of the Association for Computational Linguistics: ACL 2022*, pages 2263–2279, Dublin, Ireland, 2022. Association for Computational Linguistics.
- [17] xAI. Realworldqa. Hugging Face Datasets, 2025. Benchmark dataset for real-world spatial understanding with 700+ images and verifiable QA pairs.
- [18] Penghao Wu and Saining Xie. V*: Guided visual search as a core mechanism in multimodal llms. In *Proceedings of the IEEE/CVF Conference on Computer Vision and Pattern Recognition (CVPR)*, 2024.
- [19] Kaichen Zhang, Bo Li, Peiyuan Zhang, Fanyi Pu, Joshua Adrian Cahyono, Kairui Hu, Shuai Liu, Yuanhan Zhang, Jingkan Yang, Chunyuan Li, and Ziwei Liu. Lmms-eval: Reality check on the evaluation of large multimodal models. *arXiv preprint arXiv:2407.12772*, 2024.
- [20] Parsa Madinei, Ryan Solgi, Ziqi Wen, Jonathan Skaza, Miguel Eckstein, and Ramtin Pedarsani. Interlace: Interleaved layer pruning and efficient adaptation in large vision-language models. *arXiv preprint arXiv:2511.19676*, 2025. Submitted on 24 Nov 2025.
- [21] Simon Kornblith, Mohammad Norouzi, Honglak Lee, and Geoffrey Hinton. Similarity of neural network representations revisited. In Kamalika Chaudhuri and Ruslan Salakhutdinov, editors, *Proceedings of the 36th International Conference on Machine Learning*, volume 97 of *Proceedings of Machine Learning Research*, pages 3519–3529. PMLR, June 2019.
- [22] OpenAI. Hello gpt-4o. <https://openai.com/index/hello-gpt-4o/>, 2024. Introduction to the GPT-4o multimodal model.
- [23] Yin Xie, Kaicheng Yang, Xiang An, Kun Wu, Yongle Zhao, Weimo Deng, Zimin Ran, Yumeng Wang, Ziyong Feng, Roy Miles, Ismail Elezi, and Jiankang Deng. Region-based cluster discrimination for visual representation learning. In *ICCV*, 2025.
- [24] Xiang An, Yin Xie, Kaicheng Yang, Wenkang Zhang, Xiuwei Zhao, Zheng Cheng, Yirui Wang, Songcen Xu, Changrui Chen, Chunsheng Wu, Huajie Tan, Chunyuan Li, Jing Yang, Jie Yu, Xiyao Wang, Bin Qin, Yumeng Wang, Zizhen Yan, Ziyong Feng, Ziwei Liu, Bo Li, and Jiankang Deng. Llava-onevision-1.5: Fully open framework for democratized multimodal training. In *arxiv*, 2025.
- [25] Jia LI, Edward Beeching, Lewis Tunstall, Ben Lipkin, Roman Soletskyi, Shengyi Costa Huang, Kashif Rasul, Longhui Yu, Albert Jiang, Ziju Shen, Zihan Qin, Bin Dong, Li Zhou, Yann Fleureau, Guillaume Lample, and Stanislas Polu. NuminaMath. <https://huggingface.co/AI-MO/NuminaMath-CoT>, 2024.
- [26] Saeed Khaki, Ashudeep Singh, Nima Safaei, and Kamal Ginotra. Vistira: Closing the image–text modality gap in visual math reasoning via structured tool integration. *arXiv preprint arXiv:2601.14440*, 2026.
- [27] Edward J. Hu, Yelong Shen, Phillip Wallis, Zeyuan Allen-Zhu, Yuanzhi Li, Shean Wang, Lu Wang, and Weizhu Chen. Lora: Low-rank adaptation of large language models. *arXiv preprint arXiv:2106.09685*, 2022.
- [28] Jie Ren, Samyam Rajbhandari, Jeff Rasley, Olatunji Ruwase, and Yuxiong He. Deepspeed: Extreme-scale model training for everyone. *arXiv preprint arXiv:2110.02861*, 2021.
- [29] Samyam Rajbhandari, Olatunji Ruwase, Jeff Rasley, and Yuxiong He. Zero: Memory optimizations toward training trillion parameter models. In *Proceedings of the International Conference for High Performance Computing, Networking, Storage and Analysis (SC)*, 2020.
- [30] Jeff Rasley, Samyam Rajbhandari, Olatunji Ruwase, and Yuxiong He. Deepspeed: System optimizations enable training deep learning models with over 100 billion parameters. In *Proceedings of the 26th ACM SIGKDD International Conference on Knowledge Discovery & Data Mining*, 2020.
- [31] OpenAI. Gpt-5 system card. <https://openai.com/index/gpt-5-system-card/>, 2025. Official system card detailing GPT-5 architecture, routing, and capabilities.

A Appendix

A.1 Activation Capture and Processing Details

This section provides additional details on the activation extraction pipeline used to compute layer-wise redundancy scores in Section 3.2. All activation collection was performed on frozen models without gradient tracking.

Forward-pass instrumentation. For each decoder layer ℓ , we register a pre-forward hook to capture its input hidden states H_ℓ^{in} and a post-forward hook to capture its output hidden states H_ℓ^{out} . Both tensors are collected in floating-point precision and stored on CPU memory after each forward step. No modifications are made to the model architecture or weights.

Tokenization and modality formatting. Each example consists of a single user message containing both an image and a text prompt. Images are represented using the model’s built-in visual token format (vision start tokens, image patch tokens, padding tokens, and vision end tokens). The text prompt is appended using the model’s standard chat template, including role tags and system tokens if required by the underlying model.

Pooling. To reduce storage and enable baselines to reuse activations, we compute mean-pooled representations

$$\bar{h}_\ell^{\text{in}}, \bar{h}_\ell^{\text{out}} \in \mathbb{R}^d$$

by averaging across both batch and token dimensions. These vectors preserve coarse information about layer transformations and enable methods such as CKA and Interlace to operate without access to full activations.

Domains and sample sizes. We collect activations separately for math and non-math domains. The math domain uses 5,000 image–prompt examples, while the non-math domain uses 4,000 examples, spanning captioning, entity listing, count-based VQA, and grounding tasks. These datasets are described in Section 4.1.

A.2 Prompts Used for Math and Non-Math Probing

We use a fixed set of task prompts to ensure consistent activation probing across math and non-math domains. Each prompt is paired with an image and inserted into the model’s multimodal chat template.

Math Domain Prompts

Math-CoT (Step-by-Step Reasoning)

Solve the following mathematical problem step by step. Explain your reasoning clearly and provide the final answer. Problem: Look at the math problem in the image and solve it.

Math-Direct (Answer Only)

Solve the following mathematical problem. Provide only the final answer, without explanation. Problem: Look at the math problem in the image.

Math-Rephrase (Problem Paraphrasing)

Rephrase the following math problem in simpler words, without solving it. Problem: Look at the math problem in the image.

Math-Formalize (Equation Extraction)

Convert the following math problem into a set of mathematical equations. Do not solve the equations. Problem: Look at the math problem in the image.

Math-Verify (Feasibility Assessment)

A person claims they solved the math problem in the image. Look at the problem and determine if it appears solvable. Respond with your assessment and explain briefly.

Non-Math Prompts

Captioning (Global Description)

Describe the image in one complete, factual sentence. Avoid opinions or speculation.

Entity Listing

List the main objects or entities visible in the image. Return a comma-separated list using short noun phrases.

VQA: Counting

Question: How many main objects are visible in the image? Answer with a single number.

Grounding (Referring Expression)

Identify the object referred to by the phrase “the most prominent object” and describe it briefly using one short phrase.

A.3 Interpretation of Baseline and Baseline+SFT Results

The baseline+SFT results do not represent an attempt to improve the base model’s task performance, as shown in Table 6. Instead, this brief fine-tuning stage is designed solely to *restore generation stability* after structural pruning. Because the SFT mixture is dominated by general multimodal instruction-following data rather than task-specific supervision (for example, ChartQA- or Snapask-style data), it can shift the model’s behavior away from the original pre-training distribution. As a result, baseline+SFT sometimes underperforms the purely unpruned baseline on certain datasets. This effect is expected: the SFT stage is intended to ensure that *pruned models remain functional*, not to serve as a performance booster for the unpruned checkpoints.

Table 6: Reference accuracies for unpruned baselines. “Baseline” is the base model without fine-tuning. “Baseline+SFT” is the same model after the fixed SFT procedure used for post-pruning stabilization.

Dataset	2B Base	2B Base+SFT	4B Base	4B Base+SFT
Snapask	40.47	32.83	50.75	44.96
NuminaMath	63.45	52.61	73.49	64.06
LLaVA-OneVision	59.12	62.00	67.26	68.00
ChartQA	79.72	32.60	84.00	35.12
RealWorldQA	65.23	66.93	71.50	72.29
ScienceQA	86.47	87.80	92.71	93.46
VStar	78.01	78.01	81.68	82.20

A.4 Additional Figures

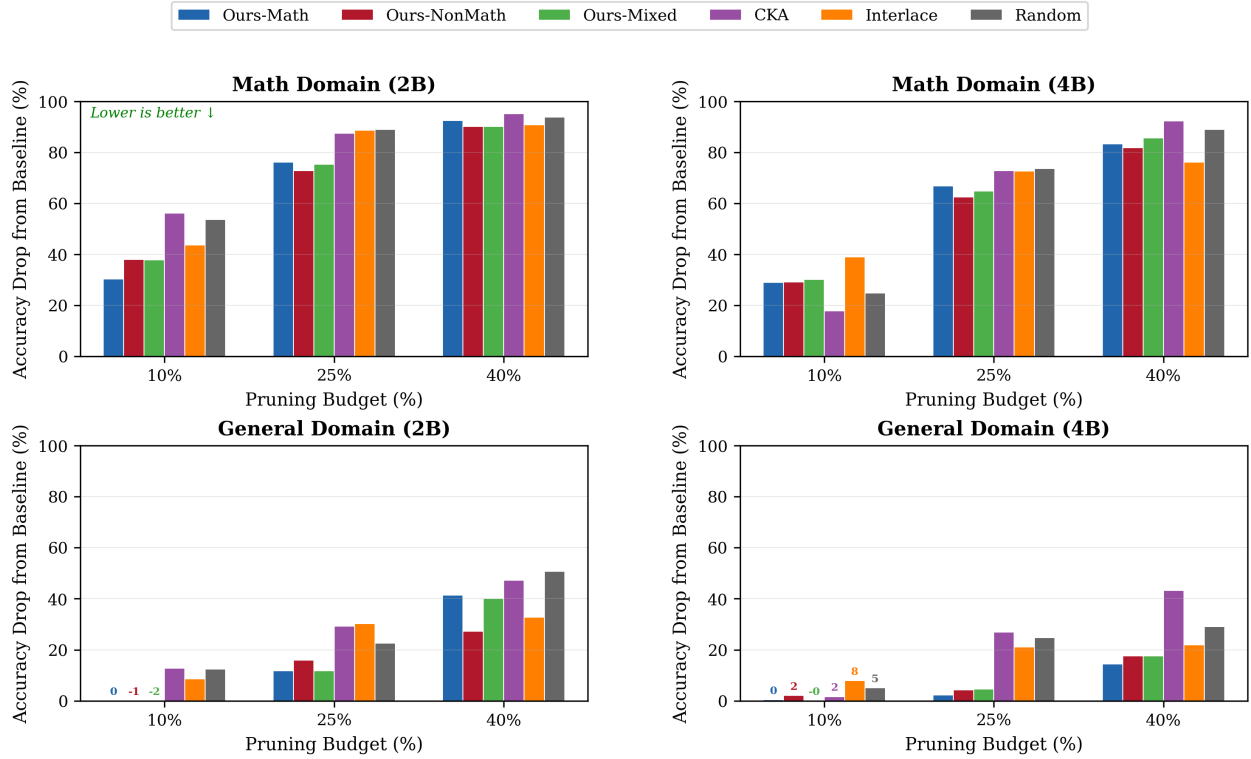


Figure 6: Relative accuracy drop from baseline by domain, model size, and pruning budget.

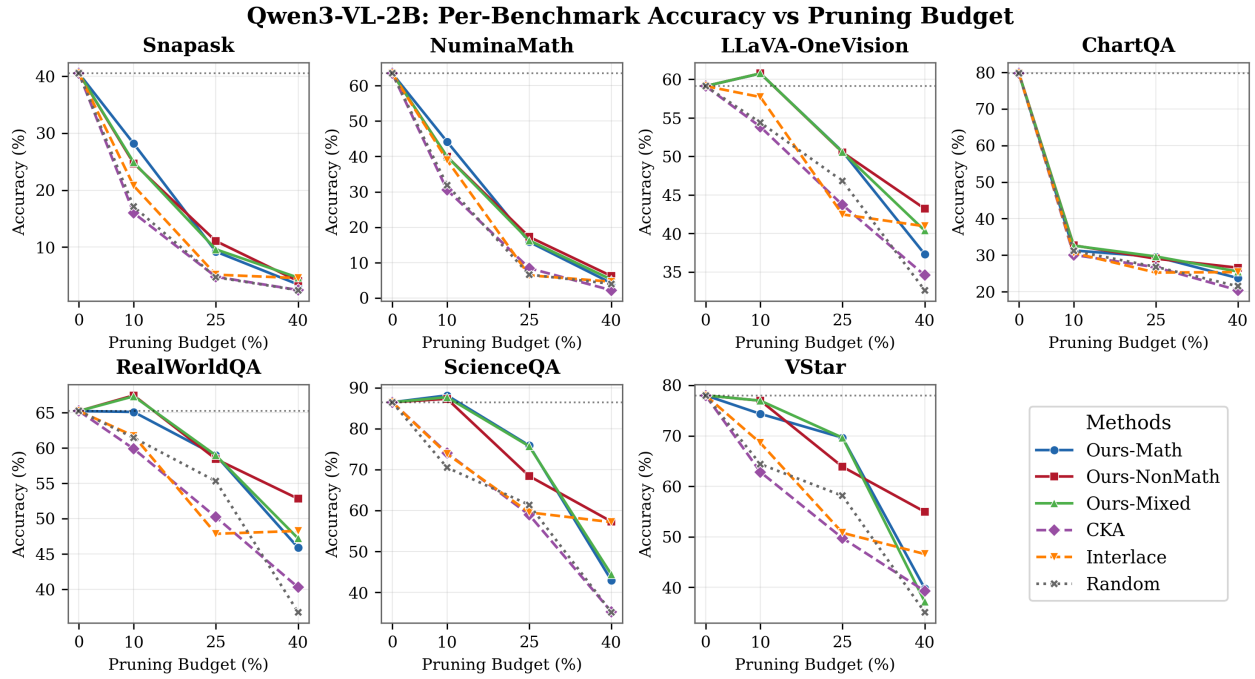


Figure 7: Per-benchmark accuracy curves for Qwen3-VL-2B.

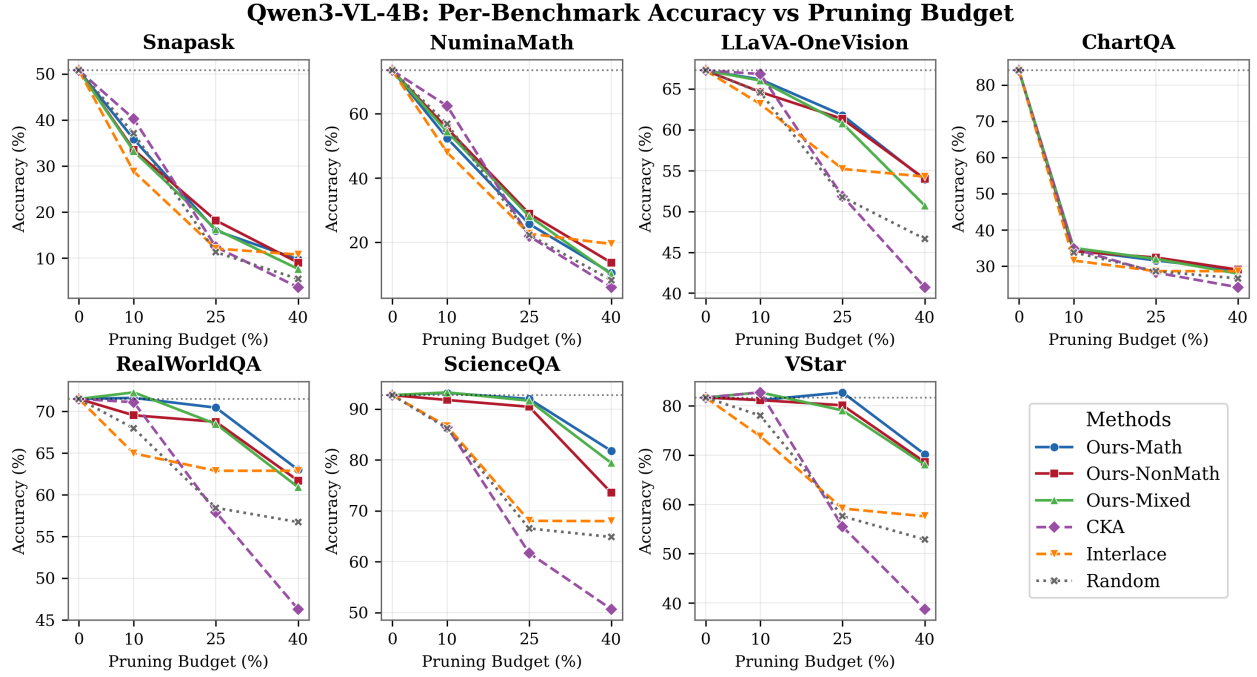


Figure 8: Per-benchmark accuracy curves for Qwen3-VL-4B.

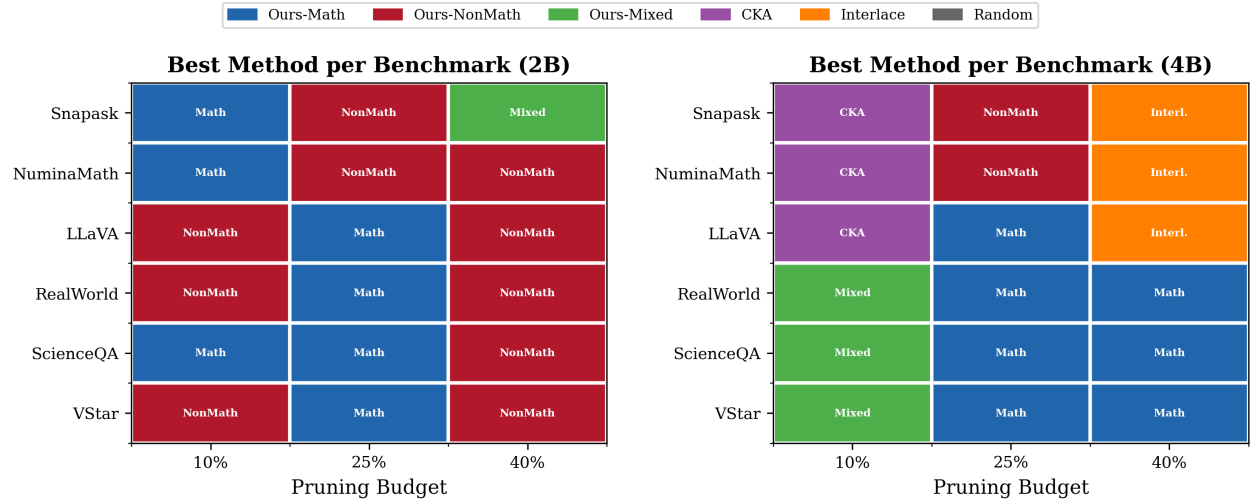


Figure 9: Best method per benchmark and pruning budget for 2B and 4B.